Monitoring the Thermal Condition of Permanent-Magnet Synchronous Motors

PEYMAN MILANFAR, Member, IEEE
SRI International

JEFFREY H. LANG, Member, IEEE
Massachusetts Institute of Technology

This paper describes a novel approach to monitoring the condition of small permanent-magnet synchronous motors (PMSM) operating under thermal stress. The approach begins with the estimation of temperature-dependent motor parameters from measurements of line voltages and currents. The parameters are then used to derive estimates of motor temperatures. Next, the electrically estimated temperatures are combined with a surface measurement of motor temperature and a dynamic thermal model of the motor to yield an observer that is a Kalman filter. The temperatures estimated by the observer are used for failure prevention. Finally, by modifying the observer, it is tuned to use the geometric properties of its innovation for failure detection. The innovation, that is, the difference between the thermally and electrically estimated temperatures, is monitored and compared against appropriate thresholds to detect failures. Failure detection is demonstrated experimentally, and shown to be capable of distinguishing the conditions of normal operation, and operation with obstructed cooling.

Manuscript received January 3, 1995; revised July 27, 1995.

IEEE Log No. T-AES/32/4/08011.

This paper is based on part of the SM thesis of P. Milanfar, Dept. of Electrical Engineering and Computer Science, Massachusetts Institute of Technology, Cambridge, MA, 1990. This work was supported by a research grant from the Omron Corporation.

Authors' addresses: P. Milanfar, SRI International, Mailstop 404-69, 333 Ravenswood Ave., Menlo Park, CA 94025; J. H. Lang, Laboratory for Electromagnetic and Electronic Systems, Dept. of Electrical Engineering and Computer Science, Massachusetts Institute of Technology, Cambridge, MA 02139.

I. INTRODUCTION

Monitoring the condition of a motor is of interest for several reasons. Firstly, during manufacturing, a monitoring system can be used to assure compliance with quality standards. Secondly, an on-line monitoring system can prevent stressful operation, thereby improving the reliability of the motor, or detect failures that may occur as a result of stressful operation, thereby increasing the reliability of the greater system. Furthermore, the analysis underlying the design of a monitoring system can yield hard limits on the physical capabilities of the motor, and hence improve the possibility of reliably using a smaller motor to perform a more demanding task.

This paper specifically develops a monitoring system for small permanent-magnet synchronous motors (PMSM) operating under thermal stress. The monitoring system is based on a thermal model of the motor. There has been considerable work on the development of such models; examples of this work can be found in [6, 19, 22]. However, this work has either concentrated on static thermal models, or has not used dynamic information to formally detect and/or prevent failures. The work presented here is *not* intended as a contribution to failure detection *theory*. Rather, in this work, we present results of our study of a particularly important *application* of this theory. Namely, the use of a dynamic thermal model along with the estimation of temperature-dependent electrical parameters in an observer structure that detects anomalous thermal behavior in small industrial motors. This, we believe, forms the basis for a novel thermal monitoring system for electric motors.

The estimation of temperature-dependent parameters in the electrical model of a motor provides a noninvasive way of estimating the temperature within the motor. Such estimates are referred to here as *electrically estimated* temperatures. By themselves, these estimates may not be sufficiently accurate to serve as reliable indicators of thermal stress or thermally induced failures. Alternatively, a dynamic thermal model of the motor, driven by models of losses in the motor, may also be developed to provide noninvasive temperature estimates. Such estimates are referred to here as *thermally estimated* temperatures. By themselves, these estimates may also not be sufficiently accurate to serve as reliable indicators of thermal stress or thermally induced failures. However, the errors within the electrically estimated temperatures and the thermally estimated temperatures should be sufficiently different that a thermal observer which combines both estimates and a measurement of motor surface temperature could produce internal temperature estimates which are sufficiently accurate for thermal condition monitoring. This is the principal conclusion of this work.

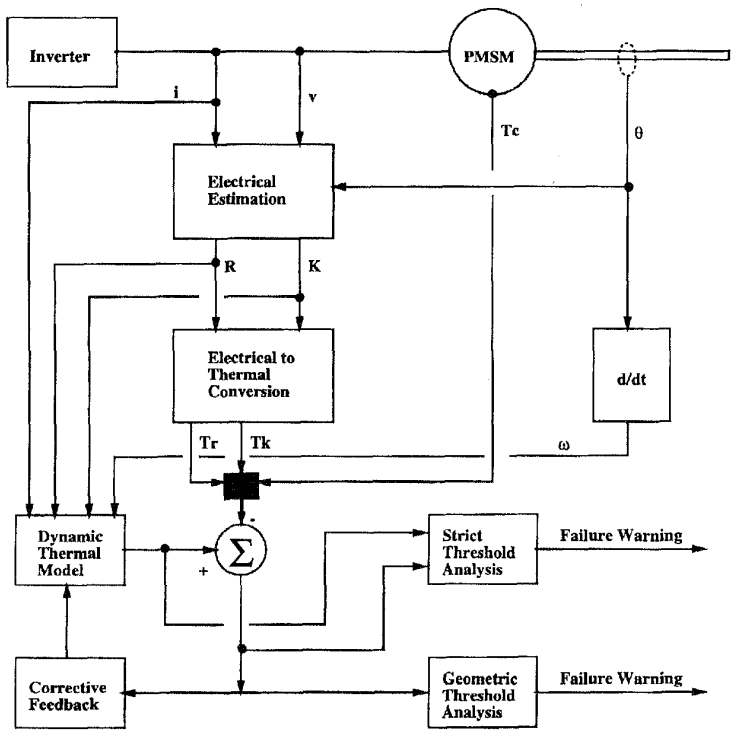

Fig. 1. Thermal condition monitoring system.

A general failure monitoring system of the type developed here is shown in Fig. 1. Measurements of motor line voltages, line currents, and position are combined to estimate an average phase resistance and permanent magnet strength. These parameters are then used to estimate the average temperature of the phases and the magnets. This is described in Sections II and III. Next, measurements of motor line currents and velocity are combined with the estimated electrical parameters to model losses in the motor. These losses form the input to a dynamic thermal model. This is also described in Section II. Next, the thermal model, the electrically estimated temperatures, and a directly measured surface temperature are combined to form an observer, which is designed to be a Kalman filter. This is described in Section III. Finally, the observer gains are modified so that the innovation in the observer can be easily monitored, and compared against thresholds to detect various failures. This is also described in Section III. Experiments based on the thermal monitoring system shown in Fig. 1 are described in Section IV.

The experimental motor studied here is manufactured with samarium-cobalt magnets, the strength of which does not change significantly with temperature. Therefore, the more general thermal condition monitoring system shown in Fig. 1 is reduced, in what follows, to eliminate T_K and the use of magnets as internal thermometers. However, in those cases where the magnet strength is a useable function of temperature, the magnets should be reinstated as internal thermometers.

II. MODELING

This section presents both the electrical and thermal models of the PMSM studied here.

A. Electrical Model

The electrical model of the PMSM assumes three balanced phases wound with a single harmonic, and connected in a wye or delta configuration. Given this assumption, the electrical dynamics of the PMSM in the rotor frame are modeled by

$$\begin{bmatrix} L_d & 0 \\ 0 & L_q \end{bmatrix} \frac{di}{dt} = -Ri + N\omega \begin{bmatrix} 0 & L_q \\ -L_d & 0 \end{bmatrix} i - NK\omega \begin{bmatrix} 0 \\ 1 \end{bmatrix} + v \tag{1}$$

where v is the two-axis voltage, i is the two-axis current, ω is the rotor velocity, R is the phase resistance, L_d and L_q are the direct-axis and quadrature-axis inductances, respectively, K is the permanent magnet strength, and N is the number of magnetic pole pairs in the motor [18]. Note that the voltage and current vectors are further defined

by

$$v = [v_d \quad v_q]', \qquad i = [i_d \quad i_q]' \tag{2}$$

where $'$ denotes algebraic transposition. Both v and i can be readily determined from measurements of the motor line voltages and currents, and rotor position θ [18].

The temperature-dependent parameters in (1) are the phase resistance R, and the magnet strength K. In general, both parameters can be used as "thermometers." The phase resistance is temperature dependent because the conductivity of copper is a function of temperature [5]. The magnet strength is usually temperature dependent (e.g., samarium-cobalt being an exception) because the magnetization of the permanent magnets is a function of temperature.

B. Thermal Model

On the basis of experimentation, it was determined that the PMSM studied in the experiments reported here exhibits linear dynamic thermal behavior with two prominent states [21]. One state is primarily associated with the temperature of the aggregated stator and rotor core, while the second is primarily associated with the phases[1] Additionally, it is observed that the motor has three independent internal sources of heat. These are losses in the phases, the stator and rotor core, and the bearings. Since the motor is manufactured with thermally insensitive samarium-cobalt magnets, we use a thermocouple measurement (T_c), made at the surface of the motor, to better capture the thermal dynamics of the stator and rotor core.

Given the characteristics of the experimental motor, it is appropriate to use a second-order dynamic thermal model with the temperatures of the thermocouple and phases serving as the two states. An appropriate thermal model is then

$$T = [T_c \quad T_r]' \tag{3}$$

$$\frac{dT}{dt} = AT + Bu \tag{4}$$

where T_c and T_r are the thermocouple and phase temperature rises *above ambient*, respectively, A and B are 2×2 and 2×3 matrices, respectively, and u is a vector related to the heat sources. We have more to say about the structure of A and B later.

The three primary losses in the motor are in the phases, the core and the bearings. Consequently, u can be modeled by

$$u = \begin{bmatrix} u_r \\ u_c \\ u_b \end{bmatrix} = \begin{bmatrix} R(T_r)i'i \\ \omega^2((L_d i_d + K)^2 + L_q^2 i_q^2) \\ \omega \end{bmatrix}. \tag{5}$$

Note that u_c is proportional to the square of the phase flux linkage and the motor velocity. Therefore, core losses are modeled primarily as resulting from eddy currents. Note further that u_r is dependent on T_r through R.

It is convenient to eliminate the coupling between u and T. To do so, make use of the definitions

$$R = R_{\text{amb}} + CT_r \tag{6}$$

$$J = \begin{bmatrix} 0 & B_{11}Ci'i \\ 0 & B_{21}Ci'i \end{bmatrix} \tag{7}$$

$$u_r^* = R_{\text{amb}} i'i \tag{8}$$

where R_{amb} is R at the ambient temperature T_{amb}, and C is the temperature coefficient of R. Then, (4) may be replaced by

$$\frac{dT}{dt} = (A + J)T + Bu^* \tag{9}$$

in which u^* differs from u only in that u_r is replaced by u_r^*, and the matrices A and B in (9) are the same as in (4).

The thermal model of (9) can be inverted to determine the maximum permitted steady-state i_d and i_q for a specified temperature rise. These current limits can in turn be used to determine the maximum steady-state torque which the motor can produce for a specified temperature rise. This information is useful in sizing a motor to a given task.

The matrices A and B in (4) must be determined before the thermal model is useful. For the motor studied in the experiments reported here, A and B are determined experimentally. To do so, the motor is thermally exercised in several different ways: it is heated through its phases with $\omega = 0$; it is driven at different speeds with $i = 0$; and it is operated normally over a wide range of loads. The transient and steady-state data for all experiments are combined and used to formulate a constrained least-square-error estimate of the parameters within A and B based on techniques described in [1, 2]. During these experiments, T_r is actually measured by first measuring R, and then converting this measurement according to the dependence of the resistivity of copper on temperature.

The estimation of the parameters in A and B is constrained because they represent the dynamics of a thermal system. Lumped-parameter thermal systems have passive electrical resistor-capacitor networks as analogs [9]. In fact, we can directly model the thermal system in (4) as an RC circuit shown in Fig. 2 where i_{eq} denotes a current source (or heat flux) describing

[1]It should be noted that more complex thermal models of the motor can certainly be hypothesized which take into account localized variations of temperature directly. Such models would be very useful for monitoring hot spots in the motor which can cause significant damage. In our framework, we chose to concentrate on a coarser thermal model of the motor which only takes into account aggregate temperatures in the motor.

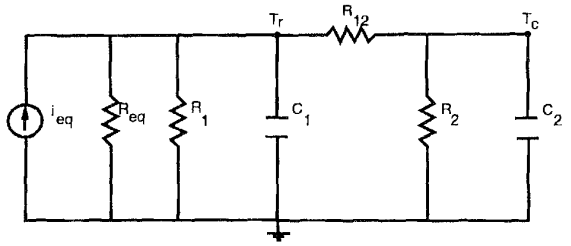

Fig. 2. *RC* circuit model for thermal system.

the thermal heat sources in the motor, while R_{eq} is intended to capture other unmodeled thermally resistive elements affecting the thermal dynamics of the motor. It is not difficult to show that with this circuit model, the matrix A has the following form:

$$A = \begin{bmatrix} -\frac{1}{C_2}\left(\frac{1}{R_{12}} + \frac{1}{R_2}\right) & \frac{1}{C_2 R_{12}} \\ \frac{1}{C_1 R_{12}} & -\frac{1}{C_1}\left(\frac{1}{R_{12}} + \frac{1}{R_1} + \frac{1}{R_{eq}}\right) \end{bmatrix}. \tag{10}$$

It can be shown that if the capacitor voltages are chosen as the states, any system matrix (such as our A), derived from a corresponding RC network, is the negative of an *M-matrix* [4, 21]. This class of matrices can be characterized by two properties [3]: 1) all diagonal entries of an M-matrix are strictly positive, while all off-diagonal entries are negative or zero, and 2) the real part of each eigenvalue of an M-matrix is positive. For 2×2 M-matrices, condition 2 amounts to the determinant of the matrix being strictly positive [3].

Instead of attempting to estimate all the unknown resistance and capacitance values within the circuit model of Fig. 2, we use the M-matrix constraints to compute a constrained least-squares estimate of the elements of A directly. Given that A is only 2×2, using the M-matrix constraints results in a reasonably simple and numerically well-conditioned estimation problem for A.

As for B, to be physically meaningful, it must have all positive elements since all thermal inputs *always* contribute to rising temperatures in the motor. This is the only constraint we impose on B when computing a least-squares estimate of it. If these constraints are not imposed on the estimation of A and B, then they must at least be used to check that the estimated A and B make physical sense.

III. CONDITION MONITORING

The essence of the thermal monitoring system is shown in Fig. 1. It consists of three parts. The first part is an estimator of temperature rises based on electrical measurements. The second part is a thermal observer based on the thermal model. The third part is a condition monitor with failure detection based on the observer output and its innovation. Each of these parts is described in the subsections which follow.

A. Electrical Temperature Estimation

In steady-state, (1) can be rewritten as

$$\begin{bmatrix} i_d \\ i_q \end{bmatrix} R = \begin{bmatrix} N\omega L_q i_q + v_d \\ -N\omega L_d i_d + v_q - N\omega K \end{bmatrix}. \tag{11}$$

Now, given measurements of v, i, ω, and K, R can be estimated by least-square-error estimation [23]. Note that v and i can be readily obtained from measurements of the line voltages, line currents, and θ, while K is assumed fixed and measured off-line. Finally, from R, estimates of T_r can be obtained.

It should be noted that the use of least-square-error estimation is somewhat out of place when applied to (11) because there is measurement noise on both sides of (11). Consequently, total least-square-error estimation is more appropriate [8]. However, because there is (relatively) much more noise on the right-hand side of (11), ordinary least-square-error estimation works quite well.

B. Thermal Observer

An observer for the thermal model of (9) can be readily developed following [20]. To do so, define the output vector y to comprise the electrical estimate of T_r and the thermocouple surface measurement of T_c. Then,

$$y = T + n \tag{12}$$

where n is a vector of measurement noise which we assume is Gaussian and white. Note that by selecting the states to be the measurable temperatures, a minimal model is obtained. Then, an appropriate thermal observer is

$$\frac{d\hat{T}}{dt} = (A + J)\hat{T} + Bu^* + G(y - \hat{T}) \tag{13}$$

where G is a matrix of gains. Note that to implement (13), both J and u^* must be determined. This involves measurements of i and ω, which will be noisy. If the measurement noise is small, then its presence can be linearized. In this case, it can be treated as an additive process input noise in the usual manner for observer development [20]. Such a simplification was found to be appropriate in the case of the measurements of the experimental motor studied here [21]. Therefore, to capture the measurement uncertainty in J and u^* to first order, the noise term Bm is then added to the right hand side of (13). This yields

$$\frac{d\hat{T}}{dt} = (A + J)\hat{T} + Bu^* + G(y - \hat{T}) + Bm. \tag{14}$$

The gain matrix G in (14) can be determined as the result of a Kalman filter design. For the sake

of simplicity, we assume that m and n are mutually uncorrelated, Gaussian, and white noise processes. In practice, the noises are surely not white and Gaussian. However, we found that this simplifying assumption was typically not a bad one [21]. The advantage of using Kalman filter gains is that they are derived from a meaningful analysis of the effects of the process and measurement noise. Alternatively, G could be designed based on a desired bandwidth for the observer.

C. Failure Prevention and Detection

One important use of the temperatures estimated by the thermal observer is the monitoring of the thermal stress on the motor, and the prevention of failures. For example, $\hat{T}$ can be monitored to determine when the insulation of the phases is at risk of thermal damage. To a certain extent, the quality of the temperature estimates can be judged from the magnitude of the residual $(\hat{T} - y)$ and its covariance. The smaller the innovation, the better the estimated temperatures, and the magnitude of the innovation indicates the probable magnitude of the estimation errors.

Perhaps a more important use of the observer and its temperature estimates is failure detection. A number of general failure detection schemes have been proposed and applied in the past with varying degrees of success [13–16]. To a large extent, the success of a particular design will depend on the nature of the particular problem at hand. In our case, the general technique of "failure-sensitive" filters, and in particular the geometric failure detection methodology [10–12] are not only useful conceptually, but they also provide detailed failure isolation information in addition to being very easy to implement on-line. In general terms, observer-based failure detection, or geometric failure detection, is based on the notion that it may be possible to design an observer so that, in the presence of a failure, its error dynamics evolve in a fixed subspace of the output space [10]. In this case, the innovation also evolves in a fixed subspace. By monitoring the innovation, and detecting its continued presence in the subspace associated with the failure, it may be possible to detect the failure.

To be specific about observer-based failure detection, consider the case of the PMSM as modeled here. Define the estimation error e according to

$$e = \hat{T} - T \tag{15}$$

and consider its evolution in the presence of a failure which is modeled as a change in the thermal state matrix from A to $A + \delta A$. Note that the failure becomes present in (9) but not in the observer (14) which is based on the (failure-free) model. Differentiating both sides of (15), and substituting the derivatives of $\hat{T}$ and T by the right-hand sides of (14) and (9) respectively, the evolution of e is determined to be

$$\frac{de}{dt} = (A + J - G)e + Bm + Gn - \delta AT. \tag{16}$$

From (16), it is apparent that when the dynamics of e are stable, the two noise processes m and n, and the failure δA drive e away from zero. Next, assume that δAT is of the form $f\eta$ where f is a constant event vector, and η is a scalar function of time. Further, assume that G is chosen so that f is an eigenvector of $(A + J - G)$. Following these assumptions, except for the stimulus of m and n, e is driven in the direction of f in the presence of the failure. Consequently, the innovation $(\hat{T} - y) = e - n$, is also driven in that direction. This forms the basis of geometric failure detection. When the innovation consistently grows sufficiently large in the direction of f so that it can be detected above the noise threshold driven by m and n, then the failure associated with δA is detected. See Fig. 5. For the second-order system considered here, a second failure can also be independently detected provided that its event vector does not point in the direction of f. This method of failure detection can be generalized greatly beyond the example discussed here [10, 21].

There is, in general, no guarantee that δAT will take the form of $f\eta$, nor is there a guarantee that G can be chosen so that f is an eigenvector of $(A + J - G)$. In some sense, the physics of the system must cooperate. In the case of the PMSM, however, both assumptions hold. For example, if the cooling of the PMSM is obstructed, this can be captured reasonably well (and experimentally verified) as an increase in the value of R_{eq} in (10). This, in turn, yields the event vector $f = [0\ 1]'$. An independent event vector $f = [1\ 1]'$ results if the motor is placed in an elevated ambient temperature.

The choice of the observer gain G is now complicated by the dual purposes of the observer, namely failure prevention and detection. For the former purpose, Kalman filter gains are appropriate since optimal estimates of temperature are sought after. For the latter purpose, however, it is necessary to assign the eigenvectors of $(A + J - G)$. To satisfy both needs, we can have a bank of filters, one for each purpose. Here, however, we only concentrate on the design of the filter for the latter purpose of failure detection, but try to maintain robustness to noise. The approach we take to this detection problem is to de-tune the Kalman filter gains so that the observer becomes a suboptimal state estimator with the desired eigenvectors [10]. In particular, we proceed as follows.

Write the eigen-decomposition of the error dynamics as

$$A + J - G = U\Sigma U^{-1} \tag{17}$$

where the columns of U are the eigenvectors of the left-hand side and Σ is a diagonal matrix containing the eigenvalues of the same. Now assume that the gain is

specified by a Kalman filter design; $G = G_k$. We then have

$$A + J - G_k = U_k \Sigma_k U_k^{-1}. \tag{18}$$

Next, form the matrix U_d whose columns are two linearly independent event vectors of two failures of interest. We then choose the observer gain G such that

$$A + J - G = U_d \Sigma_k U_d^{-1} \tag{19}$$

or

$$G = A + J - U_d \Sigma_k U_d^{-1}. \tag{20}$$

In this way, the eigenvalues of the error dynamics $A + J - G$ are taken from the Kalman filter design and the eigenvectors are those required for failure detection. This method, although ad-hoc, provides an effective way of adaptively updating the filter response in the presence of changing *noise* statistics while maintaining its failure detection capabilities.

To carry out failure detection, it is necessary to determine when the error has grown significantly in the direction of f. Thus, a threshold must be chosen for comparison. The structure of the observer provides a simple way to select such a threshold by making use of the error covariance matrix of the observer [7, 21]. This matrix can be computed dynamically, or a steady-state matrix can be used. In either case, the observer need not be a Kalman filter for this to work. The thresholds used in the experiments reported here are computed this way with 3 standard deviations being selected as the threshold magnitudes. Fig. 5 illustrates this failure detection. It shows the two-dimensional innovation space, the two independent event vectors, the detection threshold, and the background innovation noise which is nominally within the threshold. Failures are detected when the innovation exceeds the detection threshold for a given period of time. Which failure is detected depends on which way the innovation vector points with respect to the two event vectors. It should be noted that the statistically optimal approach [16], which yields smaller false alarm rates, would be to calculate the likelihood ratios from the residuals and compare these against a threshold for detection purposes. However, this approach is more computationally expensive than the one we have proposed. In effect, we have sacrificed some performance to gain some computational savings. To regain some of the lost performance, we filter the residuals using a median filter [17] before comparing them to the threshold. Since the median filtering operation can be effected very efficiently, the overall detection scheme is fast and tends to perform well as we show in the next section.

IV. EXPERIMENTS

The motor used in the experiments has a rated torque and speed of 0.636 Nm and 3000 rpm. Its peak torque rating is 1.908 Nm. Further, it is characterized by $N = 3$, $R = 1.82$ Ohms, $K = 0.092$ Vs/rad, $L_d = 9.17$ mH, $L_q = 8.4$ mH, and

$$A = \begin{bmatrix} -4.8 & 1.17 \\ 8.6 & -14 \end{bmatrix} \times 10^{-4}$$

$$B = \begin{bmatrix} 0.2212 & 0.0022 & 0.0097 \\ 1.5781 & 0.0076 & 0.0055 \end{bmatrix} \times 10^{-3}$$

where A and B are given in SI units. Using this motor, three types of experiments are performed as described below.

In the experiments described below, the motor was run at a variety of speeds and against a variety of loads, sometimes during a thermal transient and sometimes during steady-state. In all experiments, line voltages and currents, ω, θ, R, and T_c were all measured. From the line voltages and currents, and θ, v, and i were computed, and from R, T_r was computed.

A. Electrical Estimation

To study the electrical estimation of T_r, R was estimated from the collected data following the method of Section III. Then, T_r was determined from the estimated R, and compared against T_r determined from actual measurements of R. Throughout, K was assumed to be constant. In general T_r was consistently estimated to within 4°C by this procedure, and often with greater accuracy. It was observed that the estimation errors were greatest at higher speeds where the speed voltage was a dominant term in (1). This was directly a consequence of the (multiplicative) terms ωi_d and ωi_q on the right-hand side of (11). Namely, any error in the measurement of i_d and i_q is severly amplified by the magnitude of ω, particularly at higher speeds.

The absence of the speed voltage at lower speeds, however, made it difficult to estimate K should this have been desirable. The optimal speed range for the estimation of both parameters was observed to be in the vicinity of 1000 to 2000 rpm with a large load applied to the motor.

B. Thermal Observation

The thermal observer designed in Section III was tested by comparing its temperature estimates against the measured temperatures. In the case of T_r, the temperature measurement was derived from a measurement of R. In all experiments, G was designed as a Kalman filter gain. In preparation for this, the covariance matrices for m and n were experimentally found to be, respectively,

$$Q = \begin{bmatrix} 0.078 & 0 \\ 0 & 0.2925 \end{bmatrix} \quad (^\circ\text{C})^2 \tag{21}$$

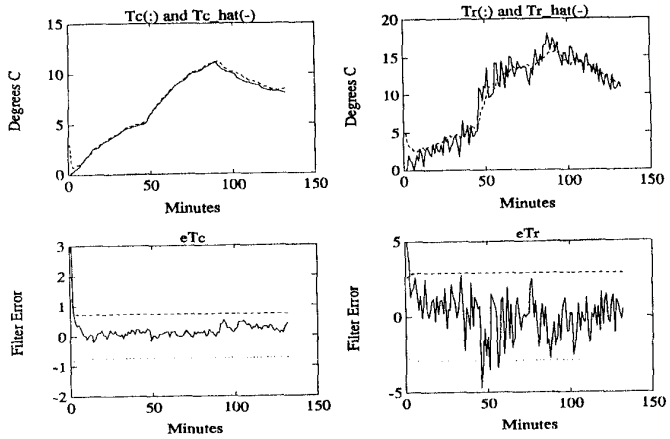

Fig. 3. Thermal observation in the absence of failure. Left-hand graphs display T_c, right-hand graphs display T_r. Top graphs display temperature rises. Bottom graphs display innovations.

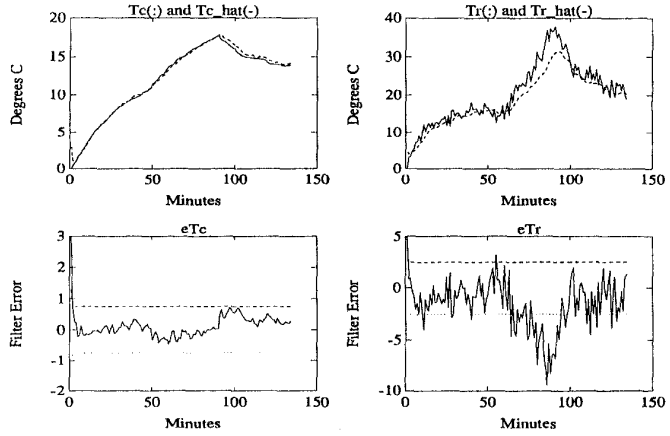

Fig. 4. Detection of cooling failure with $f = [0\ 1]'$. Some form as Fig. 2.

$$S = \begin{bmatrix} 0.2 & 0 \\ 0 & 3.5 \end{bmatrix} \quad (^\circ\mathrm{C})^2. \tag{22}$$

The covariance matrix Q was determined by using the degree of accuracy provided by the measurement equipment, while the process noise covariance S was experimentally derived based on the size of the unmodeled thermal phenomena in the motor. It was further experimentally determined that the measurement noise covariance matrix varies with the phase resistance R; R in turn grows with temperature and the temperature is typically greatest at high speeds. Hence, an accurate representation of the disturbances would relate S to the operating speed of the motor. In the interest of simplicity, a constant value for S was employed.

The results of a typical transient experiment are shown in Fig. 3. In general, the estimates of T_c and T_r were always within 0.5°C and 2°C, respectively. The dashed curve is the estimated temperature, and the solid curve is the electrically estimated temperature; their difference is the innovation. In this experiment, the velocity and the load torque were stepped up from 1500 r/min and 0.18 Nm to 2500 r/min and 0.275 Nm after 45 min of operation. They were returned to their original values after 90 min of operation. The figure also shows the estimation error. Note that the error consistently remains within three standard deviation as determined by the design of the Kalman filter. Three standard deviations above and below zero error are shown by dashed and dotted lines, respectively, around the innovations.

C. Failure Detection

An example of failure detection is shown in Fig. 4 which has the same form as Fig. 3. In this experiment, the speed and the load torque remained at 2500 r/min and 0.275 Nm, respectively. After 45 min of operation, the motor was wrapped in insulating styrofoam. This created a thermal failure whose event vector was approximately $[0\ 1]'$. After 90 min of operation, the insulation was removed.

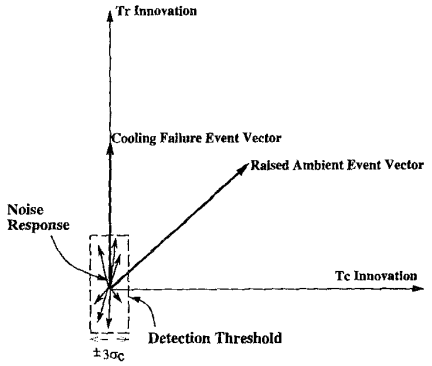

Fig. 5. Geometric failure detection.

Given an event vector in the $[0\ 1]'$ direction, the innovation should grow in the $[0\ 1]'$ direction. Thus, the innovation should remain small for T_c, but grow large for T_r. Here, large and small may be defined by the standard deviation of the observer in the presence of normal noise, but in the absence of a failure. The failure caused by the insulation is clearly visible in the figure. Between 45 and 90 min of operation, the estimation error for T_c remains within three standard deviations while the estimation error for T_r grows outside of this threshold. Thus the failure was easily detected. Successful experimental results for the detection of failures induced by raised ambient temperature ($f = [1\ 1]'$) are also reported in [21]. Note that postprocessing of the failure signature would enhance its visibility against the standard deviation thresholds [21]. This in turn reduces the chances of false alarms and missed detections. One particularly useful form of postprocessing for this application employed in [21] is the median filter [17].

V. SUMMARY AND CONCLUSIONS

This paper presented a thermal condition monitoring system for small PMSMs. The system was capable of supporting both thermal failure prevention and detection. The system was based on electrically and thermally estimated temperatures which were combined in a thermal observer. The estimated temperatures, which were accurate to within several °C, were used for condition monitoring, while geometric analysis of the innovation in the observer was used for failure detection. Both were demonstrated experimentally. In summary, the failure detector was capable of distinguishing between normal operation, and operation with obstructed cooling. The principal conclusion, then, was that motor temperatures could be estimated with sufficient accuracy to support successful condition monitoring and failure detection.

REFERENCES

[1] Moonen, M., De Moor, B., Vandenberghe, L., and Vandewalle, J. (1989)
On- and off-line identification of linear state-space models.
International Journal of Control, **49**, 1 (1989), 219–232.

[2] Nelson, L., and Stear, E. (1976)
The simultaneous on-line estimation of parameters and states in linear systems.
IEEE Transactions on Automatic Control, (Feb. 1976), 94–98.

[3] Poole, G., and Boullion, T. (1974)
A survey on M-Matrices.
SIAM Review, **16**, 4 (Oct. 1974).

[4] Wyatt, J. L., Jr., Zukowski, C. A., and Penfield, P., Jr. (1985)
Step response bounds for systems described by M-matrices, with applications to timing analysis of digital MOS circuits.
In *Proceedings of the 24th Conference on Decision and Control*, Ft. Lauderdale, FL, Dec. 1985.

[5] Chemical Rubber Co. (1986)
Handbook of Chemistry and Physics, Chemical Rubber Company, Cleveland, OH, 1986.

[6] Cho, K. R., Lang, J. H., and Umans, S. D. (1989)
Detection of broken rotor bars in induction motors using state and parameter estimation.
In *Proceedings of IAS Annual Meeting*, (1989), 1–6.

[7] Gelb, A. (1988)
Applied Optimal Estimation (10th ed.).
Cambridge, MA: MIT Press, 1988.

[8] Golub, G., and Van Loan, H. (1989)
Matrix Computations (2nd ed.).
Baltimore, MD: Johns Hopkins University Press, 1989.

[9] Holman, J. P. (1982)
Heat Transfer (5th ed.).
New York: McGraw-Hill, 1982.

[10] Jones, H. (1973)
Failure detection in linear systems.
Ph.D. dissertation, Department of Aeronautics and Astronautics, Massachusetts Institute of Technology, Cambridge, MA, 1973.

[11] Beard, R. V. (1971)
Failure accomodation in linear systems through self-reorganization.
Report MVT-71-1, M.I.T. Man Vehicle Laboratory, Cambridge, MA, Feb. 1971.

[12] Massoumnia, M. A. (1986)
A geometric approach to the synthesis of failure detection filters.
IEEE Transactions on Automatic Control, **AC-31**, 9 (Sept. 1986).

[13] Willsky, A. S. (1976)
A survey of design methods for failure detection in dynamic systems.
Automatica, **12** (1976), 601–611.

[14] Isermann, R. (1984)
Process fault detection based on modeling and estimation methods—A survey.
Automatica, **20**, 4 (1984), 387–404.

[15] Basseville, M., and Nikiforov, I. V. (1993)
Detection of Abrupt Changes—Theory and Applications.
(Information and Systems Science Series).
Englewood Cliffs, NJ: Prentice-Hall, 1993.

[16] Willsky, A. S., and Jones, H. L. (1976)
A generalized likelihood ratio testing approach for the detection and estimation of jumps in linear systems.
IEEE Transactions on Automatic Control, **AC-25** (1976), 347–360.

[17] Giardina, C. R., and Dougherty, E. R. (1988)
Morphological Methods in Image and Signal Processing.
Englewood Cliffs, NJ: Prentice-Hall, 1988.

[18] Kraus, P. (1986)
Analysis of Electric Machinery.
New York: McGraw-Hill, 1986.

[19] Lindsay, J. F., and Barton, T. H. (1972)
A modern approach to induction machine parameter identification.
IEEE Transactions on Power Apparatus and Systems, **91** (1972), 1493–1500.

[20] Luenberger, D. G. (1979)
Introduction to Dynamic Systems.
New York: Wiley, 1979.

[21] Milanfar, P. (1990)
Failure monitoring in permanent-magnet synchronous motors.
SM Thesis, Department of Electrical Engineering and Computer Science, Massachusetts Institute of Technology, Cambridge, MA, 1990.

[22] Perez, I. J., and Kassakian, J. G. (1979)
A stationary thermal model for smooth air gap rotating electric machines.
Electric Machines and Electromechanics, **3** (1979), 285–303.

[23] Strang, G. (1980)
Linear Algebra and its Applications (2nd ed.).
New York: Academic Press, 1980.

Peyman Milanfar (S'90—M'93) received his B.S. in engineering mathematics from the University of California at Berkeley in 1988, and his M.S., E.E., and Ph.D. degrees in electrical engineering from the Massachusetts Institute of Technology, Cambridge, in 1990, 1992, and 1993, respectively.

In 1993 he joined ALPHATECH, Inc. as a member of the technical staff, where he carried out research in multiresolution image processing and compression, and Over-The-Horizon radar signal processing. Since July 1994, he has been with SRI International's Applied Electromagnetics and Optics Laboratory, where his current research interests are in statistical signal and image processing as applied to problems in motion estimation, anomaly detection, and nondestructive evaluation.

Dr. Milanfar is a member of Sigma Xi and the Mathematical Association of America.

Jeffrey H. Lang (S'78—M'80) received the B.S., M.S., and Ph.D. degrees in electrical engineering from the Massachusetts Institute of Technology, (M.I.T.) Cambridge, in 1975, 1977, and 1979, respectively. From 1977 through 1979 he held a Fannie and John Hertz Foundation Fellowship. In 1980, Dr. Lang joined the Department of Electrical Engineering and Computer Science at M.I.T. where he is now Professor of Electrical Engineering. His research involves the analysis, design, and control of physical systems, and currently concentrates on electromechanical systems with application to traditional electric machine systems, micro sensors and actuators, and flexible structures.

Dr. Lang is a member of Eta Kappa Nu and Tau Beta Pi.